

# FitEM2EM—Tools for Low Resolution Study of Macromolecular Assembly and Dynamics

Ziv Frankenstein<sup>1</sup>, Joseph Sperling<sup>2</sup>, Ruth Sperling<sup>3</sup>, Miriam Eisenstein<sup>4\*</sup>

**1** Department of Structural Biology, Weizmann Institute of Science, Rehovot, Israel, **2** Department of Organic Chemistry, Weizmann Institute of Science, Rehovot, Israel, **3** Department of Genetics, The Hebrew University of Jerusalem, Jerusalem, Israel, **4** Department of Chemical Research Support, Weizmann Institute of Science, Rehovot, Israel

## Abstract

Studies of the structure and dynamics of macromolecular assemblies often involve comparison of low resolution models obtained using different techniques such as electron microscopy or atomic force microscopy. We present new computational tools for comparing (matching) and docking of low resolution structures, based on shape complementarity. The matched or docked objects are represented by three dimensional grids where the value of each grid point depends on its position with regard to the interior, surface or exterior of the object. The grids are correlated using fast Fourier transformations producing either matches of related objects or docking models depending on the details of the grid representations. The procedures incorporate thickening and smoothing of the surfaces of the objects which effectively compensates for differences in the resolution of the matched/docked objects, circumventing the need for resolution modification. The presented matching tool *FitEM2EM<sub>IN</sub>* successfully fitted electron microscopy structures obtained at different resolutions, different conformers of the same structure and partial structures, ranking correct matches at the top in every case. The differences between the grid representations of the matched objects can be used to study conformation differences or to characterize the size and shape of substructures. The presented low-to-low docking tool *FitEM2EM<sub>OUT</sub>* ranked the expected models at the top.

**Citation:** Frankenstein Z, Sperling J, Sperling R, Eisenstein M (2008) *FitEM2EM—Tools for Low Resolution Study of Macromolecular Assembly and Dynamics*. PLoS ONE 3(10): e3594. doi:10.1371/journal.pone.0003594

**Editor:** Che John Connon, University of Reading, United Kingdom

**Received:** July 10, 2008; **Accepted:** October 9, 2008; **Published:** October 31, 2008

**Copyright:** © 2008 Frankenstein et al. This is an open-access article distributed under the terms of the Creative Commons Attribution License, which permits unrestricted use, distribution, and reproduction in any medium, provided the original author and source are credited.

**Funding:** ZF is partially supported by the Kimmelman Center for Macromolecular Structure and Assembly at the Weizmann Institute of Science. JS and RS thank the US NIH, grant GM079549. The funding source had no role in the design and execution of the computations or in the analyses of the results or the preparation of the manuscript.

**Competing Interests:** The authors have declared that no competing interests exist.

\* E-mail: miriam.eisenstein@weizmann.ac.il

## Introduction

The structures of large and flexible macromolecules and macromolecular assemblies are hard to determine and the current experimental techniques often produce only medium to low resolution models. Single particle electron microscopy (EM) is one such technique that produces models at resolutions as high as 4 Å [1,2]. Other techniques that produce low resolution structures are atomic force microscopy (AFM) [3,4] and small angle X-ray scattering (SAXS) [5,6]. Recently, single particle EM in vitrified ice (cryo-EM) was used to study the structural heterogeneity of macromolecules and assemblies, exploiting the fact that the fast vitrification traps samples at different conformations and different stages of activity [7–9]. Characterizing and analyzing structural heterogeneity of macromolecules is challenging as it requires comparison of low resolution models obtained at different resolutions and sometimes using different techniques, each carrying its typical experimental error. Currently such comparisons are customarily done by manual fitting of the models (e.g. [10–13]). Similarly, manual fitting is commonly used in assembly modeling studies (e.g. [14–16]).

Many programs that match atomic structures to EM maps have been previously presented (reviewed in [17]) however these tools were not tested for matching of one EM map to another. A computerized tool for comparing low resolution 3D models is evidently necessary. It is however a non-trivial task because maps at resolutions lower than 15 Å do not carry enough features for density comparison [18–20]; in addition experimental error,

density cutoff uncertainty and resolution differences must be considered [18,21]. Recently it was shown that the combination of shape matching with maximization of density overlap provides a superior tool for matching atomic resolution models to EM maps in the resolution range of 12–25 Å (high-to-low resolution matching) [22]. We present here new tools designed for comparing and matching low resolution models (*FitEM2EM<sub>IN</sub>* for low-to-low resolution matching) and for docking of such models (*FitEM2EM<sub>OUT</sub>*). The tools are based on the shape complementarity algorithm, MolFit [23]. Hence, we employ three dimensional (3D) grid representations of the low resolution objects and use fast Fourier transformations (FFT) to match or dock them. We tested *FitEM2EM<sub>IN</sub>* on ten pairs of related EM maps and found that it can efficiently match EM maps obtained at different resolutions and using different EM techniques. Moreover, models of different conformers were successfully matched and partial structures were fitted into larger assemblies. The difference between the grid representations of the matched models can be used to study conformation changes or to predict the shape and size of substructures. Docking of low resolution EM maps with *FitEM2EM<sub>OUT</sub>* identified the expected positions and ranked them at the top of the list of predicted models.

## Results

The matching and docking tools *FitEM2EM<sub>IN</sub>* and *FitEM2EM<sub>OUT</sub>* test many relative orientations of the matched/docked

objects. The EM maps were therefore represented as ensembles of spheres (“virtual atoms”) that can be easily rotated and translated. The spheres fill the objects’ envelopes at the selected electron density cutoff values. The representation of the EM objects is governed by the parameter  $w$ , which determines the extension of the surface layer of the object and its outer shape. This parameter is likely to be affected by the resolution of the EM map and the density cutoff; its optimization was executed by matching several EM structures, each to its copy (self-matching). We chose to match symmetrical or pseudo-symmetrical EM structures expecting several correct matches (the actual number depends on the symmetry) some of which are identity matches and other are approximate either because the symmetry of the structure is not perfect or because the symmetry operation does not comply with the rotational step employed in the scan and only nearby orientations are sampled.

### Self-matching of EM maps

Nine EM structures determined at different resolutions (from 11.2 to 42.2 Å) and obtained using different experimental procedures were selected for this test (see Table 1). EM maps were taken from the Macromolecular Structure Database (EMDB) at <http://www.ebi.ac.uk/msd-srv/emsearch>. The electron density cutoffs were obtained from the investigators in most cases; in other cases the cutoffs were manually approximated to reproduce the published EM objects.

Several rotation-translation matching scans were performed for each structure in the benchmark, employing different  $w$  values. The rotations interval was fixed at  $12^\circ$  in these tests. The highest score in each scan was either that of the identity match (no rotation; translation within 3 grid steps of the expected position) or of an exact symmetry related match. Matches that deviate by  $\sim 6^\circ$  (half the rotation step) from a correct position (identity or

symmetry related) were ranked after the exact symmetry matches and were followed by matches that deviate by  $\sim 12^\circ$  (the rotations grid interval). In only one case, the SV40 T antigen, a false match, rotated by  $180^\circ$  about an axis perpendicular to the  $C_6$  symmetry axis, was ranked among the matches with  $\sim 12^\circ$  deviation; this is a false match because the SV40 T antigen does not have  $D_6$  symmetry even at the low resolution of 29 Å. The score of this false match is however only 54% of the score of the top ranked correct match.

The optimal  $w$  for each map was chosen based on 2 criteria: the first was good tolerance of deviations up to  $6^\circ$  from a correct position, thus the scores of such matches were close to the score of the identity match ( $\geq 80\%$ ). The second criterion was that deviations of  $12^\circ$  were tolerated yet were distinct from the correct matches; hence the scores of these matches were positive but dropped to  $\sim 15\%$ – $70\%$  of the score of the identity match. It appears that ranges of  $w$  comply with these criteria for each system (see Table 2), which is indicative of only moderate sensitivity of the matching results to  $w$ . However, the  $w$  ranges vary considerably between systems and  $w$  is negatively correlated with the EM map grid interval ( $R^2 = 0.85$  for the central values of the  $w$  ranges) and with the resolution ( $R^2 = 0.78$ ; see Figure 1). This is expected, because the optimal  $w$  were chosen to confer limited tolerance of structural mismatches the extent of which depends on the experimental resolution and the grid interval. In contrast,  $w$  is not correlated with the density cutoff ( $R^2 = 0.16$ ). This is also expected, because the density cutoff used to produce the molecular envelope depends on the molecular volume and on the background scattering of the electrons beam hence on the EM method and the experimental conditions [21,24].

Unlike  $w$ , the virtual atoms radii (determined by  $w$  and  $g$ , see Methods) are not correlated with the resolution (see Table 2). The average virtual atoms radius calculated with the central values of

**Table 1.** Benchmark of EM structures used in the optimization of  $w$ , the parameter that determines the width and shape of the surface layer of object A.

System	EMDB code	EM method/complex symmetry	Resolution <sup>a</sup> (Å)	Optimal $w$ range	R1 <sup>b</sup>	R2 <sup>c</sup>
ATP-7ClpB mutant [10]	1244	cryo-EM/ $C_6$	11.2	3.2–3.6	9.4	8.6
TET1 peptidase [42]	1188	cryo-EM/tetrahedral 12-mer	14	2.6–3.0	10.4	10.6
apo-7ClpB [10]	1241	cryo-EM/ $C_6$	17.7	3.0–3.4	9.2	8.0
TIP48/TIP49 complex [43]	1317	uranyl acetate negative staining/ $C_6$	20	2.0–2.2	9.9	11.3
GroES-ADP <sub>7</sub> -GroEL-ATP <sub>7</sub> [27]	1046	cryo EM/ $C_7$	23.5	1.8–2.2	8.1	9.0
MCM helicase [44]	1134	uranyl acetate negative staining/ $C_6$	25	1.8–2.2	10.1	10.9
SV40 T antigen [45]	1024	uranyl acetate negative staining/ $C_6$	29	1.8	10.3	11.0
DnaB [25]	1022	cryo-EM/ $C_3$	34.5	1.6–2.0	10.3	9.7
DnaB.DnaC complex [25]	1023	cryo-EM/ $C_3$	42.2	1.4	8.8	7.9
DnaB.DnaC complex at two resolutions [25,26]	1023/1017	cryo-EM/ $C_3$	34.1	1.8–2.0	10.4	9.5
GroES-ADP <sub>7</sub> -GroEL-ATP <sub>7</sub> and GroES-ATP <sub>7</sub> -GroEL [27,28]	1046/1180	cryo EM/ $C_7$	15.6	2.2–2.6	6.7	7.8
ATP-7ClpB mutant and ADP-7ClpB [10]	1244/1242	cryo-EM/ $C_6$	14.0	2.6–3.0	8.2	8.4
AMPPNP-7ClpB and ADP-7ClpB [10]	1243/1242	cryo-EM/ $C_6$	14.4	3.0–3.4	9.4	8.4
GroES-ADP <sub>7</sub> -GroEL-ATP <sub>7</sub> and GroEL-ATP <sub>7</sub> [27]	1046/1047	cryo-EM/ $C_7$	19.2	2.6–3.0	8.4	8.1

<sup>a</sup>The resolution quoted here is the value in the EMDB; average resolution is given for the pairs of related structures.

<sup>b</sup>R1 is the virtual atoms radius calculated with the central values of the  $w$  ranges in column 5.

<sup>c</sup>R2 is the virtual atoms radius calculated with  $w$  values derived from the linear dependency of  $w$  on the resolution (Figure 1).

doi:10.1371/journal.pone.0003594.t001

**Table 2.** Matching related EM maps.

System <sup>a</sup>	EMDB code and resolution (Å)	$w$ and $g$	No. of matches and correct matches with score > -10000	Rank of highest ranking false match
DnaB.DnaC complex [25]	1023, 42.2	1.7	277	39
DnaB.DnaC complex [26]	1017, 26.0	3.75	38	
GroES-ADP <sub>7</sub> -GroEL-ATP <sub>7</sub> [27]	1046, 23.5	2.8	57	24
GroES-ATP <sub>7</sub> -GroEL [28]	1180, 7.7	2.11	27	
GroES-ADP <sub>7</sub> -GroEL-ATP <sub>7</sub> [27]	1046, 23.5	2.6	21	17
GroEL-ATP <sub>7</sub> [27]	1047, 14.9	2.35	18	
GroES-ATP <sub>7</sub> -GroEL [28]	1180, 7.7	3.2	915	20
GroES-ATP <sub>7</sub> -(single-ring)GroEL [29]	1286, 10.4	1.79	29	
ATP-7ClpB mutant [10]	1244, 11.2	2.9	145	66
ADP-7ClpB [10]	1242, 16.7	2.22	89	
AMPPNP-7ClpB [10]	1243, 12.1	2.9	84	73
ADP-7ClpB [10]	1242, 16.7	2.25	72	
AMPPNP-7ClpB [10]	1243, 12.1	3.0	12	3
ATP-7ClpB mutant [10]	1244, 11.2	2.22	12	
TFIID-closed [30] <sup>b</sup>	1194, 33.0	1.7	1	13
TFIID-open [30]	1196, 35.0	5.12	1	
apo-ORC [31] <sup>b</sup>	1252, 34.0	1.7	39	14
ATP-ORC [31]	1253, 34.0	5.26	13	
Ribosome 80S [32] <sup>b</sup>	1093, 18.3	2.4	262	3
Ribosome 40S [32]	1092, 25.3	3.69	3	

<sup>a</sup>The first structure in each pair is the stationary object A and the second structure is the moving object B.

<sup>b</sup>Values are given for matching with the lowest density cutoff for object A and highest cutoff for object B (see text).

doi:10.1371/journal.pone.0003594.t002

the  $w$  ranges is  $9.6 \text{ \AA} \pm 0.8$ . The corresponding average calculated with  $w$  derived from the dependency graph in Figure 1 is  $9.7 \text{ \AA} \pm 1.3$ . It appears that the optimal  $w$  values modify the resolution of the EM map creating surfaces that are not resolution dependent. Virtual atoms with radius of  $9.7 \text{ \AA}$  produce a surface that confers tolerance to small structural mismatches or to mispositioning due to the stepwise scanning of the rotation-translation space. This result is very important in view of the wide resolution range of EM structures.

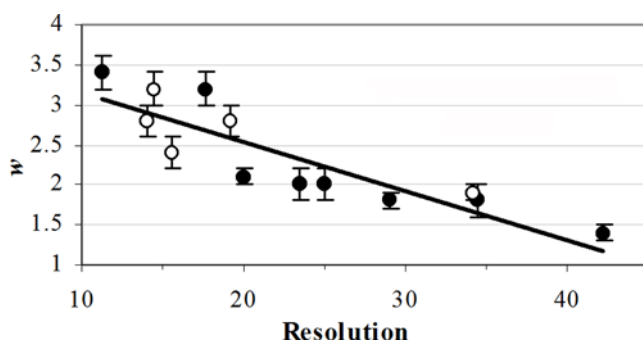


**Figure 1.** The dependency of the optimal  $w$  values on the resolution of the matched EM maps. The full circles depict the results of self-matching (for systems listed in Table 1). The hollow circles depict the results of matching of related EM maps (the average resolution is used here). The regression line ( $y = -0.0612x + 3.7551$ ;  $R^2 = 0.78$ ) is based only on the full circles. The error bars reflect the range of the optimal  $w$ .

doi:10.1371/journal.pone.0003594.g001

The search volume in these simple tests, in which objects A and B are identical, consists of the outer part of the surface layer of object A, corresponding to the difference between the surface extensions applied to the two objects. The thickness of this layer,  $(w-1)g$ , depends on the EM map resolution. Therefore, self-matching of the higher resolution EM maps, which often are presented at small grid intervals, leads to a shift of the highest scoring model at the identity orientation from the expected position ( $\leq 3$  grid steps). The best matching results are obtained when  $w > 1$  thus allowing some freedom for object B to move and adjust to object A.

### Matching related EM maps

A more realistic test of the *FitEM2EMIN* algorithm was the matching of related EM maps, including matching of the same object determined at different resolutions, matching of partial structures and matching of different conformers. Optimal  $w$  ranges were reevaluated for five pairs of structures (see Table 1). Rotation-translation scans were performed employing several  $w$  values and ranges of optimal  $w$  were determined using the abovementioned criteria. The resultant  $w$  ranges for these five cases fit reasonably well to the regression line of  $w$  versus resolution obtained in the self-matching of EM maps, as shown in Figure 1.

Ten pairs of related EM maps were used to test our matching algorithm and to demonstrate its performance. In one case, the EM maps of the complex between helicase DnaB and its DnaC loading partner, determined at very different resolutions (26 and 42.2 Å) were matched [25,26]. Despite the large difference in resolution our algorithm ranked a correct match at the top. A false

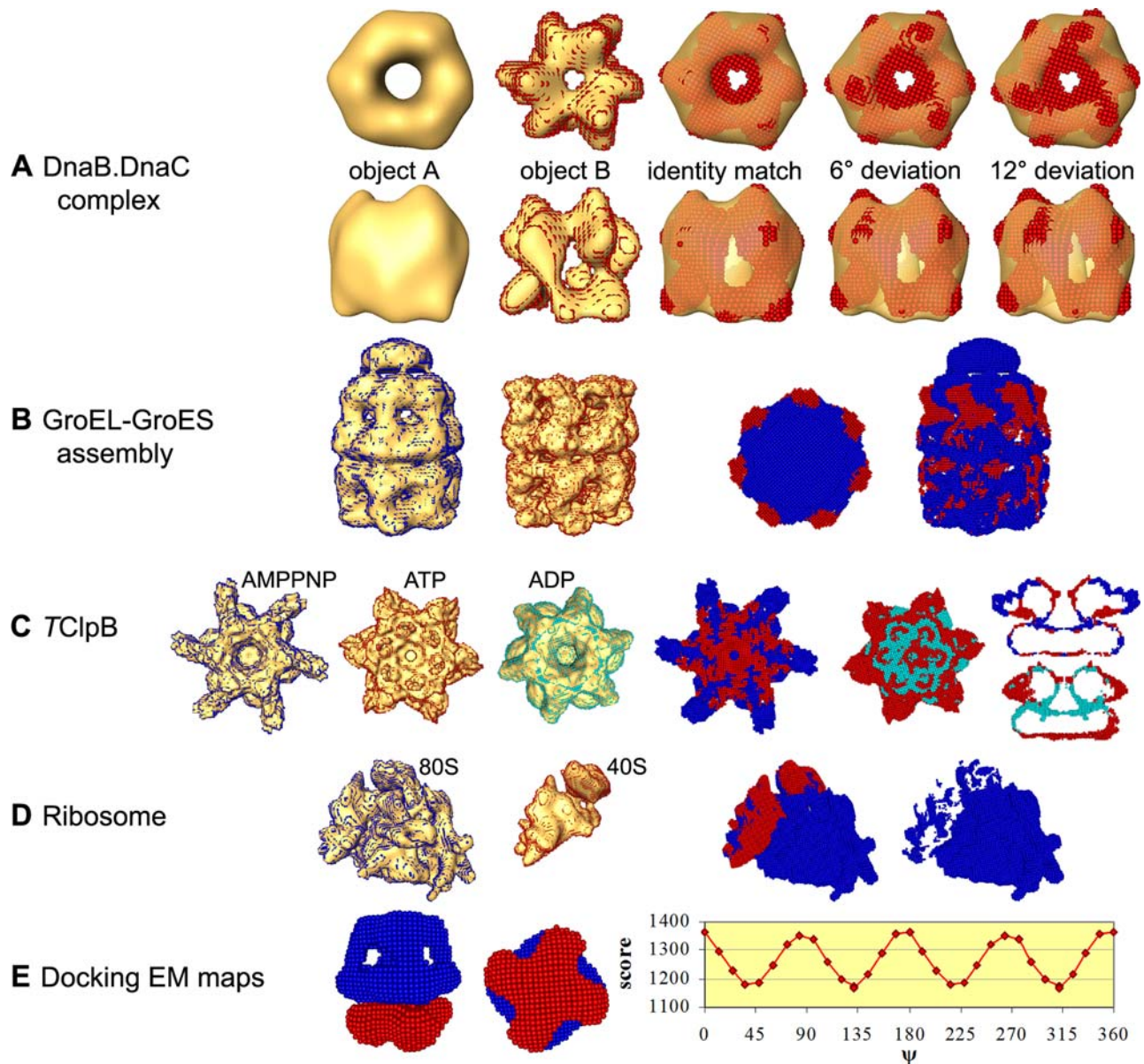


**Figure 2. Examples of low-to-low resolution matching and docking.** The top ranking matches are shown, obtained in *FitEM2EM* scans that employ  $w$  values calculated from the dependency graph in Figure 1. EM envelopes are shown in yellow. The DifferenceGrid portions where object A protrudes out of object B are colored as object A, and vice versa for object B. The individual images were prepared with the software package Amira and are not to scale. Details for each row of pictures are listed from left to right. (A) Matching of two EM structures of the DnaB.DnaC complex (top and side views). Shown are the EM envelope of objects A (resolution 42.2 Å); the virtual atoms representation of object B (resolution 26 Å) in red within its EM envelope; the identity match (score 1963, ranked 1); match deviating by 6° (score 1352, ranked 4); match deviating by 12° (score 96, ranked 7). (B) The virtual atoms representations of GroES-ADP<sub>7</sub>-GroEL-ATP<sub>7</sub> (blue) and GroEL-ATP<sub>7</sub> (red) within their EM envelopes; top and side views of the DifferenceGrid results. (C) Virtual atoms representations of AMPPNP-TClpB (blue), ATP-TClpB mutant (red) and ADP-TClpB (cyan); top views of the DifferenceGrid results for the match of AMPPNP-TClpB to ATP-TClpB mutant and for the match of ATP-TClpB mutant to ADP-TClpB; sections through the side views of the DifferenceGrid results for the same matches. (D) Virtual atoms representations of the 80S ribosome (blue) and the 40S subunit (red); the top ranking match and the DifferenceGrid results. (E) Side and bottom views of the top ranking docking model between Kv4.2\*-KChIP2 (blue) and the simulated map of β<sub>24</sub> (red); changes in the complementarity score as function of  $\psi$ , the rotation angle about the 4-fold axis of the predicted complex.

doi:10.1371/journal.pone.0003594.g002

match with a negative score is ranked 39 (see Table 2). Figure 2A presents the correct top ranking match and additional matches deviating by 6° or 12°.

The GroEL/GroES chaperonin complex is a molecular machine whose components assembly and disassembly upon ATP binding and hydrolysis is accompanied by conformation changes. GroEL consists of two 7-subunits rings, which can be in

the apo state or loaded with either ATP or ADP; GroES consists of a single 7-subunits ring. The structures of the complexes GroES-ADP<sub>7</sub>-GroEL-ATP<sub>7</sub> [27] and GroES-ATP<sub>7</sub>-GroEL [28], which were determined at very different resolutions (23.5 and 7.7 Å), are expected to be similar [28]. Our algorithm matched these objects correctly, ranking a correct match at the top. We then matched GroEL-ATP<sub>7</sub> [27] to GroES-ADP<sub>7</sub>-GroEL-ATP<sub>7</sub> [27] and the



GroES-ATP<sub>7</sub>-(single-ring)GroEL [29] to GroES-ATP<sub>7</sub>-GroEL [28]. These complexes were determined at different resolutions (see Table 2) and have different compositions; the first object in each pair is a substructure of the second. In both tests correct matches were ranked at the top despite the different assembly sizes and differences in conformation. The DifferenceGrid results for the GroEL-ATP<sub>7</sub> and GroES-ADP<sub>7</sub>-GroEL-ATP<sub>7</sub> pair highlight the conformation differences upon ATP binding to the GroEL *cis* ring (see Figure 2B) whereas the results for the GroES-ATP<sub>7</sub>-GroEL and GroES-ATP<sub>7</sub>-(single-ring)GroEL pair suggest that these two complexes are similar.

The matching of the different conformers of TClpB provided another test for the influence of conformation changes on the success rate of our procedure. TClpB is an ATP-dependant molecular chaperone which disaggregates stress-damaged proteins. Its structure consists of two hexameric rings (AAA-1 and AAA-2) rotated by 23° about the co-axial 6-fold rotation axis. It was suggested that the exposed face of the AAA-1 ring binds the substrate which is then threaded through the central pore [10]. The rings are of similar size in the ATP bound TClpB mutant (E271A, E668A) but not in apo TClpB. We note that in the self-matching of the ATP bound complex our algorithm identified a pseudo-symmetric match in which the rings interchange (rotation of 180° about an in-plane axis plus 24° about the 6-fold axis). The score of this (false) match is however only 22% of the score of the correct match. The self-docking of apo TClpB did not produce such a pseudo-symmetrical model.

We matched the ATP bound TClpB mutant and the AMPPNP and ADP bound hexamers to each other. In all three cases correct matches, similar to the manual fittings [10], were ranked at the top. The ATP- and ADP-bound TClpB matching was executed employing rotational intervals of 8, 12 or 16°, in order to test the sensitivity of the results to this parameter. A correct match was ranked at the top in every case; the scores of the top ranking models obtained in the 8° and 16° searches were slightly higher than the score obtained in the 12° search, indicating that a relative rotation of 4° marginally improves the match. This result indicates that the 12° rotation interval is adequate for identifying the correct match; yet, top ranking matches should perhaps be refined by testing small local rotations from the predicted position.

The difference between the grid representations of AMPPNP-TClpB and the top ranking matched ATP-TClpB, shown in Figure 2C, is in line with the observations of Lee et al. [10]. It highlights the extended spokes in the TClpB-AMPPNP complex compared to the shorter and thicker spokes in ATP-TClpB. There is additional density on top of the upper ring in the ATP-TClpB mutant complex and in the central pore region, making the pore narrower. The differences in the shapes of the lower ring of the two objects are minor and may be related to errors in the EM maps and in the matching. The radial spokes are even shorter in the ADP-TClpB complex and the central pore of the upper ring is narrower, in particular in the lower half. We note additional structural differences at the interface between the rings.

Two additional examples for matching of different conformers of the same molecule are the closed and open structures of the human transcription factor TFIID [30] and the apo and ATP bound Drosophila origin recognition complex (ORC) [31]. In these cases we also tested the effect of small changes in the density cutoff of the EM map on the matching results. We therefore gradually increased the volume of object A (by slightly decreasing the density cutoff value) and decreased the volume of object B (by increasing the density cutoff value). A correct match was ranked at the top in all the scans however the complementarity appeared to be better (higher scores) as the density cutoff of object A was reduced and

that of object B was increased. Notably, in both examples the EM map grid intervals and consequently the grid interval used in the *FitEM2EMIN* matching, are particularly large (>5 Å) but the identification of correct matches was not affected.

Finally we matched the 40S subunit of the human ribosome [32] to the whole ribosome (80S) assembly formed by the 40S and 60S subunits. The effect of the density cutoff change in this case was the same as described above. Thus the position of the 40S subunit within the 80S structure in the top ranked match did not change. The complementarity score however gradually increased as the density cutoff value for the 80S structure was decreased and that of the 40S structure was slightly increased, indicating that the shape and size of the 40S subunit match better within the 80S ribosome. The DifferenceGrid results (see Figure 2D) for the top ranking match can be used to approximate the shape and size of the ribosomal 60S subunit, producing a similar result to the subunits separation presented by Sphan et al. [32].

## Docking EM maps

Docking of low resolution objects is important in assembly modeling and the program *FitEM2EMOUT* was designed to perform such tasks. We could not find EM maps of substructures whose overall structure is known in order to calibrate the parameters of *FitEM2EMOUT* and test the program. Therefore, the same parameter values and grid representations as described for *FitEM2EMIN* were employed and simulated electron density maps were docked to EM maps. The simulated maps were calculated using the *pdb2vol* and *map2map* modules of *Situs* [19]. The electron density cutoff for the simulated map was chosen to encompass all the atoms in the corresponding PDB structure.

In the first test, the coordinates of the *trans* ring of GroEL [33] from PDB [34] entry 1AON were used to calculate an electron density map at 10 Å resolution (the resolution of the docking partner). This map was docked to the EM map of GroES-ATP<sub>7</sub>-(single-ring)GroEL complex [29]. Several symmetry related correct matches were ranked at the top followed by a false match (ranked 5) in which the tip of GroES makes contact with the central void of the GroEL *trans* ring. Fitting of an extreme value distribution function to the distribution of scores [35] provided estimated *E* values of  $5.6 \times 10^{-4}$  and  $2.1 \times 10^{-3}$ , respectively, for the highest ranking correct and false models.

The second test involved docking of a simulated map of the tetramer of the oxidoreductase β<sub>2</sub> subunit [36] (PDB entry 1EXB) to the EM map of the 4:4 complex between the pore-forming Kv4.2 subunits and the regulatory KChIP2 subunits [37]. The resolutions of both the EM map and the simulated electron density map were 21 Å. The β<sub>2</sub> surface that faces the T1 domain of the pore forming subunit in the T1<sub>4</sub>-β<sub>2</sub><sub>4</sub> complex [36] is expected to make contact with Kv4.2\*-KChIP2 [37]; indeed this general position of the simulated map of β<sub>2</sub><sub>4</sub> is observed in many high ranking docking models. These models differ in the rotation angle of the β<sub>2</sub> tetramer about the 4-fold symmetry axis and the docking scores change periodically as function of this angle (see Figure 2E). The score difference between the best and worst positions is within 3σ. The highest scoring false model, in which the symmetry axis of β<sub>2</sub><sub>4</sub> is not aligned with that of Kv4.2\*-KChIP2, is ranked 35. The *E* values for the highest ranking correct and false models are  $5.12 \times 10^{-6}$  and  $1.39 \times 10^{-3}$ , respectively.

## Discussion

The recent upsurge of low resolution structures obtained by different experimental techniques and the capability to study global structural changes by cryo electron microscopy, introduced

a need for computational methods to match, compare and dock such structures. We present here tools designed for low-to-low resolution matching and docking. By extending and smoothing of the surfaces of the objects our matching procedure *FitEM2EMIN* becomes resolution independent allowing comparison or fitting of objects obtained at very different resolutions without resorting to resolution modification. Such modification (that is often used in fitting of atomic structures into EM maps) requires knowledge of the target resolution, the experimental determination of which is susceptible to inaccuracies, especially in low resolution studies [38]. We show that *FitEM2EMIN* can match different conformers and fit a partial structure into a larger assembly. The procedure is not sensitive to the exact values of the parameters and ranges of  $w$  confer identification of correct and nearly correct matches and distinction from false matches. Similarly, small changes in the EM maps density cutoff affect the complementarity score but not the relative position of the matched objects or the rank of the correct match.

The success rate of *FitEM2EMIN* is excellent. Thus, in every case correct matches are obtained at the top. We attribute this success to the limited search volume (the interior plus surface of object A), which allows only few matches with positive scores. When substructures are matched into the whole structure the search volume increases considerably and the results become more similar to docking results. Thus, the number of false models obtained in the partial matching tests 80S/40S and GroES-ATP7-GroEL/GroES-ATP7-(single-ring)GroEL is higher than in most other tested cases (see Table 2). Nevertheless the difference between the scores of the correct match (top rank) and the highest ranked false match is large, facilitating distinction between them. The DifferenceGrid tool highlights major structural differences between the matched objects. In the partial docking of the 40S ribosomal subunit into the 80S ribosome this tool can be used to predict the size and shape of the 60S ribosomal subunit.

Docking is expected to produce weaker distinction between correct and false models than matching because the search space is much less limited. Nevertheless, our procedure *FitEM2EMOUT* ranked the expected docking models at the top with considerable score gap from that of the highest ranked false models.

The procedures presented here can also be used for matching of atomic resolution structures to EM maps because the large grid effectively lowers the resolution of the atomic representation of an object. In this study the electron density values were used only for determining the shape of the matched or docked objects. These values can however be used to guide the matching or docking, for example by requiring that high density regions, that may represent RNA or DNA regions, overlap. The guiding can be achieved in a similar manner to the weighting procedure previously described by our group [39]. Notably, such guided matching or docking can use experimental data regarding the positions of substructures or specific interactions, from different sources.

## Methods

### Converting EM maps into easily rotateable 3D objects

EM maps are given as 3D grids of electron density values and the objects are visualized by selecting one or more density cutoffs and drawing equi-density contours. Every EM grid point with density exceeding a selected cutoff value was listed as a virtual atom whose coordinates are those of the grid point and whose radius is  $\sqrt{3}G/2$ , where  $G$  is the EM grid interval (this representation is similar to the virtual atoms representation of the electrostatic potential by Heifetz et al. [40]). The virtual atoms thus fill the volume delimited by the selected equi-density contour.

Each virtual atom is assigned the density value of the related grid point and in this way the selected part of the EM map can be easily rotated and shifted to various positions.

### *FitEM2EMIN* – a tool for matching low resolution 3D structures

The *FitEM2EMIN* algorithm is based on the FFT docking procedure, MolFit, initially described by Katchalski-Katzir and coworkers [23]. The objects to be matched are represented by cubic grids. The center of the grid is at the centroid of the object and grid points are assigned values with regard to their position relative to the object. Grid points within the volume of any virtual atom are considered part of the object (interior or surface); other grid points are assigned “outside the object” values. Distinction between the interior and a surface layer is made for the stationary object A. The resultant grid representations are as follows:

Object A (the stationary object):

$$A_{l,m,n} = \begin{cases} \rho & \text{inside the object} \\ s & \text{on the surface of the object} \\ Oa & \text{outside the object} \end{cases}$$

Object B (the moving object):

$$B_{l,m,n} = \begin{cases} s & \text{inside the object} \\ s & \text{on the surface of the object} \\ Ob & \text{outside the object} \end{cases}$$

The grid representations are correlated using FFT, producing the matrix  $C_{\alpha,\beta,\gamma}$  (eq. 1).  $C$  holds the correlation scores for shifts of  $B_{l,m,n}$  with respect to  $A_{l,m,n}$  by  $\alpha$ ,  $\beta$ , and  $\gamma$  grid points along three perpendicular axes.

$$C_{\alpha,\beta,\gamma} = A_{l,m,n} \otimes B_{l+\alpha,m+\beta,n+\gamma} \quad (1)$$

By setting  $Oa$  to a negative value,  $s$  to a positive value and  $\rho$  and  $Ob$  to zero, the correlation scores are positive when object B is positioned within the volume of object A and overlaps its surface layer. The correlation scores reflect the degree of surface similarity between objects A and B thus higher positive scores indicate more extensive matching of the surfaces and little or no protrusion of object B outside of the volume of object A. The  $n$  highest scoring  $\alpha$ ,  $\beta$ ,  $\gamma$  shifts in the current correlation matrix are identified and saved.

To complete a six dimensional search in the rotation-translation space the moving object is rotated to a new orientation (by applying a rotation transformation to the coordinates of the virtual atoms), its grid representation is recalculated for the new orientation, and then a new correlation matrix is calculated and new high scoring positions are identified and saved. The procedure is repeated until the stepwise rotational scan is completed and then all the saved models are sorted by their correlation scores.

The surface of object A consists of at least 2 layers of voxels; it was designed such that the inner layer follows the shape of the EM object (at the selected density cutoff) and the outer layer is extended and smoothed. The extension and smoothing are achieved by increasing the virtual atoms radii to  $(\sqrt{3/2+w})g$ , where  $g$  is the *FitEM2EMIN* grid interval and  $w$  is a free parameter. A larger value of  $w$  produces a more extended and smoother outer

surface because small holes and crevices are eliminated. The surface of object B is not distinguished from its interior however the object's volume is extended and the surface is smoothed by setting the virtual atoms radii to  $(\sqrt{3/2+1})g$ .

The parameters  $s$ ,  $\rho$ ,  $Oa$ ,  $Ob$  and  $w$  determine the shapes of the objects and their grid representations; the grid interval, the rotational grid step and  $n$  are scanning parameters. Importantly, the grid interval employed in *FitEM2EMIN* is not necessarily the same grid interval as in the EM map; this freedom is made feasible by the virtual atoms representation of the EM maps that allows projection of these spheres onto cubic grids of any size. The values of  $\rho$  and  $s$  were selected to be  $-15$  and  $1$ , respectively. These values were previously determined for the high-to-high (atomic) resolution docking program MolFit [23]. The self-matching calibration tests described in the Results section show them to be adequate for low-to-low resolution matching. We chose to use a grid interval of similar magnitude to the grid interval in the experimental EM maps where possible because a smaller grid interval can create artifacts whereas a larger grid interval effectively lowers the resolution of the map. In cases when different experimental EM maps were matched, with different grid intervals, we used the average interval to reduce the error. The rotational grid interval was set to  $12^\circ$ , which was previously found to be adequate for high-to-high resolution docking [41], high-to-low resolution docking [22] and proved adequate in the calibration scans of *FitEM2EMIN*. We show in the results that use of similar rotational intervals does not affect significantly the matching results.

## References

- Mitra K, Frank J (2006) Ribosome dynamics: insights from atomic structure modeling into cryo-electron microscopy maps. *Annu Rev Biophys Biomol Struct* 35: 299–317.
- Zhang X, Settembre E, Xu C, Dormitzer PR, Bellamy R, et al. (2008) Near-atomic resolution using electron cryomicroscopy and single-particle reconstruction. *Proc Natl Acad Sci U S A* 105: 1867–72.
- Engel A, Muller DJ (2000) Observing single biomolecules at work with the atomic force microscope. *Nat Struct Biol* 7: 715–8.
- Scheuring S, Boudier T, Sturgis JN (2007) From high-resolution AFM topographs to atomic models of supramolecular assemblies. *J Struct Biol* 159: 268–76.
- Putnam CD, Hammel M, Hura GL, Tainer JA (2007) X-ray solution scattering (SAXS) combined with crystallography and computation: defining accurate macromolecular structures, conformations and assemblies in solution. *Q Rev Biophys* 40: 191–285.
- Davies JM, Tsuruta H, May AP, Weis WI (2005) Conformational changes of p97 during nucleotide hydrolysis determined by small-angle X-Ray scattering. *Structure* 13: 183–95.
- Leschziner AE, Nogales E (2007) Visualizing flexibility at molecular resolution: analysis of heterogeneity in single-particle electron microscopy reconstructions. *Annu Rev Biophys Biomol Struct* 36: 43–62.
- Frank J (2002) Single-particle imaging of macromolecules by cryo-electron microscopy. *Annu Rev Biophys Biomol Struct* 31: 303–19.
- Stark H, Luhrmann R (2006) Cryo-electron microscopy of spliceosomal components. *Annu Rev Biophys Biomol Struct* 35: 435–57.
- Lee S, Choi JM, Tsai FT (2007) Visualizing the ATPase cycle in a protein disaggregating machine: structural basis for substrate binding by ClpB. *Mol Cell* 25: 261–71.
- Taylor DJ, Nilsson J, Merrill AR, Andersen GR, Nissen P, Frank J (2007) Structures of modified eEF2 80S ribosome complexes reveal the role of GTP hydrolysis in translocation. *Embo J* 26: 2421–31.
- De Carlo S, Chen B, Hoover TR, Kondrashkina E, Nogales E, Nixon BT (2006) The structural basis for regulated assembly and function of the transcriptional activator NtrC. *Genes Dev* 20: 1485–95.
- Klaholz BP, Myasnikov AG, Van Heel M (2004) Visualization of release factor 3 on the ribosome during termination of protein synthesis. *Nature* 427: 862–5.
- Gilbert RJ, Gordiyenko Y, von der Haar T, Sonnen AF, Hofmann G, et al. (2007) Reconfiguration of yeast 40S ribosomal subunit domains by the translation initiation multifactor complex. *Proc Natl Acad Sci USA* 104: 5788–93.
- Siridechadilok B, Fraser CS, Hall RJ, Doudna JA, Nogales E (2005) Structural roles for human translation factor eIF3 in initiation of protein synthesis. *Science* 310: 1513–5.
- Rouiller I, DeLaBarre B, May AP, Weis WI, Brunger AT, et al. (2002) Conformational changes of the multifunction p97 AAA ATPase during its ATPase cycle. *Nat Struct Biol* 9: 950–7.
- Fabiola F, Chapman MS (2005) Fitting of high-resolution structures into electron microscopy reconstruction images. *Structure* 13: 389–400.
- Wriggers W, Chacon P (2001) Modeling tricks and fitting techniques for multiresolution structures. *Structure* 9: 779–88.
- Wriggers W, Milligan RA, McCammon JA (1999) Situs: A package for docking crystal structures into low-resolution maps from electron microscopy. *J Struct Biol* 125: 185–95.
- Rossmann MG (2000) Fitting atomic models into electron-microscopy maps. *Acta Crystallogr D Biol Crystallogr* 56: 1341–9.
- Frank J (1996) *Three-dimensional Electron Microscopy of Macromolecular Assemblies*. San Diego: Academic Press.
- Chacon P, Wriggers W (2002) Multi-resolution contour-based fitting of macromolecular structures. *J Mol Biol* 317: 375–84.
- Katchalski-Katzir E, Shariv I, Eisenstein M, Friesem AA, Aflalo C, et al. (1992) Molecular surface recognition: determination of geometric fit between proteins and their ligands by correlation techniques. *Proc Natl Acad Sci USA* 89: 2195–9.
- Frank J, Penczek P, Grassucci R, Srivastava S (1991) Three-dimensional reconstruction of the 70S Escherichia coli ribosome in ice: the distribution of ribosomal RNA. *J Cell Biol* 115: 597–605.
- San Martin C, Radermacher M, Wolpensinger B, Engel A, Miles CS, et al. (1998) Three-dimensional reconstructions from cryoelectron microscopy images reveal an intimate complex between helicase DnaB and its loading partner DnaC. *Structure* 6: 501–9.
- Barcena M, Ruiz T, Donate LE, Brown SE, Dixon NE, et al. (2001) The DnaB.DnaC complex: a structure based on dimers assembled around an occluded channel. *Embo J* 20: 1462–8.
- Ranson NA, Farr GW, Roseman AM, Gowen B, Fenton WA, et al. (2001) ATP-bound states of GroEL captured by cryo-electron microscopy. *Cell* 107: 869–79.
- Ranson NA, Clare DK, Farr GW, Houldershaw D, Horwich AL, et al. (2006) Allosteric signaling of ATP hydrolysis in GroEL-GroES complexes. *Nat Struct Mol Biol* 13: 147–52.
- Chen DH, Song JL, Chuang DT, Chiu W, Ludtke SJ (2006) An expanded conformation of single-ring GroEL-GroES complex encapsulates an 86 kDa substrate. *Structure* 14: 1711–22.

## FitEM2EMOUT – a tool for docking low resolution 3D structures

By setting  $s$  to a positive value,  $\rho$  to a negative value and  $Oa$  and  $Ob$  to zero, the correlation score is positive only when object B is positioned outside of and in contact with object A. The correlation score is higher when the contact area (surface overlap) is larger and there is no or very little interpenetration of the objects. The value of  $w$  optimized for the *FitEM2EMIN* procedure was used also for docking. The *FitEM2EMOUT* grid interval was made the same as the grid interval in the EM map.

## DifferenceGrid – a tool for comparing objects

This tool calculates the difference between grid representations of two objects. The virtual atoms radii of both objects are set to  $\sqrt{3/2} g$ . Grid points within object A are given the value  $s$  and the exterior is set to  $Oa$ ; the corresponding grid values for object B are set to  $s$  and  $Ob$ , respectively. The difference between the two grid representations is equal to 0 where both objects overlap and to  $Oa-Ob$  where the exterior overlap; it is equal to  $Oa-s$  where object B protrudes out of object A and to  $Ob-s$  where object A protrudes out of object B.

## Acknowledgments

We thank Sukyeong Lee, Schoehn Guy, Wendler Petra and Macias Jose R. for providing details of the density cutoffs of their EM maps.

## Author Contributions

Conceived and designed the experiments: ZF JS RS ME. Performed the experiments: ZF ME. Analyzed the data: ZF ME. Wrote the paper: ZF JS RS ME.

30. Grob P, Cruse MJ, Inouye C, Peris M, Penczek PA, et al. (2006) Cryo-electron microscopy studies of human TFIID: conformational breathing in the integration of gene regulatory cues. *Structure* 14: 511–20.
31. Clarey MG, Erzberger JP, Grob P, Leschziner AE, Berger JM, et al. (2006) Nucleotide-dependent conformational changes in the DnaA-like core of the origin recognition complex. *Nat Struct Mol Biol* 13: 684–90.
32. Spahn CM, Jan E, Mulder A, Grassucci RA, Sarnow P, et al. (2004) Cryo-EM visualization of a viral internal ribosome entry site bound to human ribosomes: the IRES functions as an RNA-based translation factor. *Cell* 118: 465–75.
33. Xu Z, Horwich AL, Sigler PB (1997) The crystal structure of the asymmetric GroEL-GroES-(ADP)<sub>7</sub> chaperonin complex. *Nature* 388: 741–50.
34. Berman HM, Westbrook J, Feng Z, Gilliland G, Bhat TN, et al. (2000) The Protein Data Bank. *Nucleic Acids Res* 28: 235–42.
35. Kowalsman N, Eisenstein M (2007) Inherent limitations in protein-protein docking procedures. *Bioinformatics* 23: 421–6.
36. Gulbis JM, Zhou M, Mann S, MacKinnon R (2000) Structure of the cytoplasmic beta subunit-T1 assembly of voltage-dependent K<sup>+</sup> channels. *Science* 289: 123–7.
37. Kim LA, Furst J, Gutierrez D, Butler MH, Xu S, et al. (2004) Three-dimensional structure of I(to); Kv4.2-KChIP2 ion channels by electron microscopy at 21 Angstrom resolution. *Neuron* 41: 513–9.
38. Stahlberg H, Walz T (2008) Molecular electron microscopy: state of the art and current challenges. *ACS Chem Biol* 3: 268–81.
39. Ben-Zeev E, Eisenstein M (2003) Weighted geometric docking: incorporating external information in the rotation-translation scan. *Proteins* 52: 24–7.
40. Heifetz A, Katchalski-Katzir E, Eisenstein M (2002) Electrostatics in protein-protein docking. *Protein Sci* 11: 571–87.
41. Eisenstein M, Shariv I, Koren G, Friesem AA, Katchalski-Katzir E (1997) Modeling supra-molecular helices: extension of the molecular surface recognition algorithm and application to the protein coat of the tobacco mosaic virus. *J Mol Biol* 266: 135–43.
42. Schoehn G, Vellieux FM, Asuncion Dura M, Receveur-Brechot V, Fabry CM, et al. (2006) An archaeal peptidase assembles into two different quaternary structures: A tetrahedron and a giant octahedron. *J Biol Chem* 281: 36327–37.
43. Puri T, Wandler P, Sigala B, Saibil H, Tsaneva IR (2007) Dodecameric structure and ATPase activity of the human TIP48/TIP49 complex. *J Mol Biol* 366: 179–92.
44. Gomez-Llorente Y, Fletcher RJ, Chen XS, Carazo JM, San Martin C (2005) Polymorphism and double hexamer structure in the archaeal minichromosome maintenance (MCM) helicase from *Methanobacterium thermoautotrophicum*. *J Biol Chem* 280: 40909–15.
45. San Martin MC, Gruss C, Carazo JM (1997) Six molecules of SV40 large T antigen assemble in a propeller-shaped particle around a channel. *J Mol Biol* 268: 15–20.